Available online at www.sciencedirect.com
ScienceDirect
Polymer 48 (2007) 2453–2459
polymer
www.elsevier.com/locate/polymer

Computer-built polyethylene spherulites for mesoscopic Monte Carlo simulation of penetrant diffusion: Influence of crystal widening and thickening

A. Mattozzi [a], M. Minelli [b], M.S. Hedenqvist [a], U.W. Gedde [a,*]

[a] School of Chemical Science and Engineering, Fibre and Polymer Technology, Royal Institute of Technology, SE-100 44 Stockholm, Sweden
[b] DICMA, School of Engineering, University of Bologna, I-40131 Bologna, Italy

Received 29 August 2006; received in revised form 9 February 2007; accepted 9 February 2007
Available online 20 February 2007

Abstract

An algorithm able to mimic crystal lengthening, branching, widening and thickening was developed in order to build spherulites similar to those observed in polyethylene. The ranges of volume crystallinity and crystal width-to-thickness ratio attainable were ≤40% and 8–35, respectively. An on-lattice Monte Carlo-based algorithm was used to generate penetrant trajectories in the built spherulites. Diffusivity was assessed from the mean-square displacement of the penetrant molecules, normalized with respect to the mean-square displacement of the penetrant molecules in a crystal-free system, and compared with the geometrical impedance factor calculated from the Fricke theory using morphological data samples in the simulated spherulites. The crystal blocking effect was greater in the tangential plane than along the spherulite radius. All data, except that for the highest crystallinity system (40%), conformed to a linear relationship between the geometrical impedance factor obtained from the diffusivity data and the geometrical impedance factor calculated from morphological data; the latter being calculated according to the Fricke model using averages based on the squares of the crystal width-to-thickness ratio data. This finding suggests that wide crystals had a more pronounced effect on the geometrical impedance factor than was indicated by their number fraction weight. The system with the highest volume crystallinity (40%) showed a markedly higher geometrical impedance factor than predicted by the Fricke theory using the two aforementioned modifications.

Keywords: Diffusion; Spherulite; Simulation

1. Introduction

Diffusion of small-molecule penetrants in semicrystalline polymers is retarded compared to that in their amorphous analogues because the penetrant molecules must bypass the impermeable crystals. Most models quantify the effect of the penetrant detour in terms of a geometrical impedance factor (τ_{DIFF}) defined according to [1]:

$$\tau_{DIFF} = \frac{D_a}{D \times \beta} \quad (1)$$

where D is the penetrant diffusivity in the semicrystalline polymer, D_a is the penetrant diffusivity in the fully amorphous analogue, and β is a factor taking into account the constraining effect of the crystals on the amorphous component. The purpose of the present paper was to study the effect of morphological factors on the penetrant detour ignoring the constraining effect of the crystals on the amorphous component. This means that β was set to unity in all the calculations executed.

Different attempts have been made to predict the detour effect of the crystals from morphological data. Michaels and Bixler [1] derived an analytical expression to calculate the geometrical impedance factor from crystal structure data based on the Fricke model [2] originally derived for the electrical conductivity of two-component systems. Michaels and Bixler sketched

* Corresponding author. Tel.: +46 8 7907640; fax: +46 8 208856.
E-mail address: gedde@polymer.kth.se (U.W. Gedde).

0032-3861/$ - see front matter © 2007 Elsevier Ltd. All rights reserved.
doi:10.1016/j.polymer.2007.02.041

the structure of semicrystalline polymers in simple terms, where the polymer consists of impenetrable oblate spheroid crystals embedded in a penetrable amorphous phase. The model suggests that the geometrical impedance factor is determined only by the volume crystallinity (v_c) and the crystal width-to-thickness ratio (W/L_c). Müller-Plathe et al. [3] and Hadgett et al. [4] used a mesoscopic Monte Carlo simulation of penetrant diffusion in a generic semicrystalline polymer consisting of isolated platelets, equiaxed in the fold surface plane, embedded in an amorphous matrix. These models clearly resembled the Michaels and Bixler model. They do not, however, resemble the superstructural crystal arrangement of polymer spherulites with dendritically branching crystal lamellae that are essentially continuous from the centre to the periphery of the spherulite.

This study is a continuation of a previous paper [5] that presented data on penetrant diffusion in computer-built polyethylene-spherulite-like structures. This paper was to our knowledge the first of its kind. The spherulites were obtained by starting from an initial single crystal block and allowing crystal growth along the crystallographic *b*-axis on the two opposite lateral faces. Crystallisation occurred only on the active lateral faces by adding crystal blocks with a specified width (W), thickness (L_c) and length along the growth direction (gs). Crystal lengthening proceeded until impingement occurred. In order to obtain the continuous three-dimensional crystalline structure observed in polymer spherulites [6–11], lamellar branching and splaying were introduced by simulation using random numbers. On-lattice Monte Carlo simulations of penetrant diffusion were used to obtain the penetrant diffusivity according to the Einstein equation. The crystallinity dependence of the geometrical impedance factor at a given crystal width-to-thickness ratio was linear, which is in general accordance with the Fricke model. However, analysis of the penetrant trajectories showed that the Fricke theory underestimated the crystal blocking effect by neglecting the fact that the crystals were longer along the spherulite radius than in any other direction. It must be stressed that these findings were obtained for samples within a limited volume crystallinity range, 21–35% [5]. The initial model was based on several simplifying assumptions: (1) the crystal ribbons had constant predefined values for width and thickness; (2) crystals were infinitely stiff, which means that a crystal that impinges with another crystal always stops its growth; and (3) the limitations in the number of lattice points used restricted the attainable volume crystallinity range to $\leq$35%. In the present study, the first assumption has been relaxed allowing crystal growth along the crystallographic *a*- and *c*-axes. Hence, the built spherulites consist of crystals with a distribution in the crystal width-to-thickness ratio. A positive side effect of the relaxing condition was that structures with a moderately higher degree of crystallinity were attainable.

2. Theory and simulations

2.1. Spherulite growth: crystal widening and thickening

The simulations were performed on MATLAB R13 running on a PC. A single initial crystal was placed in a corner of a cubic lattice and the spherulite growth was allowed to take place inside a spherical octant centred in the initial crystal and inscribed in the cubic lattice: the final primary structure was therefore a spherulite octant. The full spherulite was then built on the basis of the primary octant by mirror-imaging of the structure generating seven mirror-image octants.

Mattozzi et al. [5] presented details about the algorithm used for the simulation of crystal lengthening and branching. A brief recapitulation of the method described in the previous paper follows. The initial crystal block had a specified initial length (dimension along *b*; 1, 2 or 3 lattice units), width W_i (dimension along *a*; 4 or 10 lattice units were used in the different simulations) and thickness L_{ci} (dimension along *c*; 1, 2 or 4 lattice units were used in the different simulations). The crystal growth was according to the previous paper only allowed along the *b*-axis. The branching of the crystal was controlled by random numbers using a preset probability value for branching ($P_b = 0.4$ was used in this study). The branching process was controlled by five parameters. (i) Splay angle (Sy), which is the angle between the growth-vector of the branching (daughter) lamella projected on the plane of the original (mother) lamella and the growth-vector of the mother lamella. This parameter was set to 20° or 40°. (ii) Split angle (St), which is the angle between the growth-vector of the daughter lamella and the projection of this vector on the plane of the mother lamella. This parameter was set to 15° or 30°. (iii) The branching lamella undergoes twisting, i.e. the crystallographic *c*-axis rotates about the crystal growth-vector. The twisting was prescribed by three parameters (universal values given with parentheses were used in the simulations): initial torsion angle (2°), total torsion angle (20°) and torsion length (12 lattice units). The chosen values of split and splay angles consented to obtain highly crystalline structures with uniform crystallinity within the built octant in accordance with findings presented in a previous study [5].

The crystal growth occurred within predefined shells; shell by shell were added to finally obtain the final spherulite octant structure. The crystal growth within each shell occurred by two separate mechanisms. The primary growth occurred first according to the aforementioned principles. The desired degree of crystallinity was obtained by filling the remaining free space with secondary lamellae branching out from the primary lamellar structure. The secondary growth process was the tool to control the crystallinity within each shell and the algorithm determined the crystallinity within each shell and if this value was within ±10% of the average crystallinity, the growth was allowed. Otherwise, the growth of the shell was regenerated.

The following new elements were added to the algorithm used in the previous study [5]: the number of active faces for crystal growth was increased from the previous 2 to 4 when both lengthening and widening processes were considered and to 6 when lengthening, widening and thickening processes were considered. The crystal growth occurred in discrete steps. Crystal lengthening was simulated by adding an element with the same width and thickness as the initial crystal and with a predefined length gs. As in the first model [5], the crystalline

elements were defined by a set of numbers referred to as 'key points' stored in the matrix 'kps'. In addition to global position, local coordinate system, lengthening direction and growth log, the present model considered data for the width and thickness of the crystal unitary blocks. Crystal widening and thickening occurred by increasing the width and the thickness of the single crystalline elements using discrete quantities referred to, respectively, as gsw and gst. The two directions of crystal widening and thickening were processed separately. Crystal lengthening, widening and thickening proceeded until impingement with other crystals occurred. Widening and thickening occurred either simultaneously (parallel model) or subsequent to (series model) crystal growth along *b* and branching. Parallel widening steps are displayed in Fig. 1a–c: a widening step (Fig. 1b) is completed at each lengthening step (Fig. 1c).

The points in the cubic lattice were given values of either one or zero, depending on whether they were located within or outside the crystalline volume and the values were stored in a matrix referred to as 'box3D'. The matrix was used for calculating the volume crystallinity and for simulating penetrant diffusion. The lattice consisted of 9×10^6 sites.

2.2. Simulation of penetrant diffusion

An on-lattice random walk, based on a Monte Carlo process, was used to simulate penetrant diffusion. The walk was enabled in a sphere, built from the primary octant structure (Section 2.1), defined by $[x, y, z] \in [-r; r]$, x, y and z being the Cartesian coordinates of the penetrant and r the radius of the spherulite. Periodic boundary conditions were introduced to obtain a continuous system of impinged spheres: a penetrant molecule intersecting the sphere boundary re-entered on the diametrically opposite position of the sphere. The direction of each move was determined by a random number generator in order to have equiprobable moves to the nearest neighbour lattice site. The generic step to $[x, y, z]$ was accepted if the lattice site with coordinates $[|x|, |y|, |z|]$ in the spherulite was amorphous and rejected otherwise, but the move counter was still updated. A correction was introduced for the degeneration of points having coordinates equal to zero. Both the Cartesian and the spherical coordinates of the penetrant were saved. The penetrant trajectory used for the diffusivity calculation was obtained by unwrapping the coordinates of the walk.

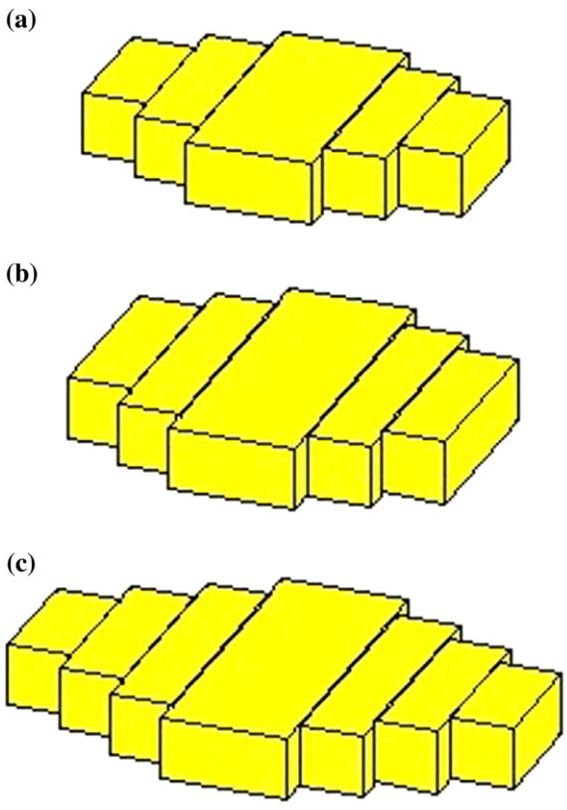

Fig. 1. The crystallisation process: the initial structure (a) undergoes a lateral growth step (b), followed by a lengthening step (c).

2.3. Calculation of penetrant diffusivity and geometrical impedance factor

Penetrant diffusivity D was calculated from the displacement vector $\mathbf{r}$ at time t according to [12]:

$$D = \frac{\lim_{t\to\infty} \left\langle (\mathbf{r}(t) - \mathbf{r}(0))^2 \right\rangle}{2dt} \tag{2}$$

where d is the dimensionality of the diffusion system. The applicability of Eq. (2) is limited to time scales in which the mean-square displacement is based on data with statistical significance. The geometrical impedance factor (τ_{DIFF}) was calculated from Eq. (1), where D is the penetrant diffusivity in the built spherulite and D_a is the diffusivity in an identical lattice without crystals; the factor β was set to unity in all the calculations.

3. Results and discussion

3.1. Volume crystallinity and crystal width-to-thickness ratio

Table 1 presents input data for the spherulite-builder together with two characteristic features (volume crystallinity and crystal width-to-thickness ratio) of the resulting spherulitic structure. These data show a moderate but still significant increase in the crystal width-to-thickness ratio from the initial values (2–5) to the final values ranging between 4.5 (5) and 9 (10); the values within parentheses refer to the averages based on the squared values of the parameter. A lowering in the lateral growth rate with respect to the growth rate along the *b*-axis had a significant impact on the final crystal width-to-thickness ratio (Table 1, cf. rows 3 and 4). Another general tendency, also reported previously for spherulites based on crystals with a uniform crystal width-to-thickness ratio [5], was that spherulites based on crystals with low crystal width-to-thickness ratio generally showed a high crystallinity (Table 1).

Fig. 2 shows a fully developed spherulite octant. Crystalline elements added in lateral growth are shown in a darker (red)

Table 1
Input parameters used in the simulations and crystallinity and average crystal width-to-thickness ratio of built spherulites

r[a]	d, t, w[b]	gs, gsw, gst[c]	St[d]	Sy[e]	v_c[f]	$\langle W/L_c \rangle$[g]	$\sqrt{\langle (W/L_c)^2 \rangle}$[h]
174	1, 2, 4	1, 1, 0	15	20	40.2	4.59	5.56
182	1, 2, 4	1, 1, 0	15	20	27.3	6.42	7.84
174	1, 2, 4	1, 1, 0	15	20	29.4	6.18	7.61
174	1, 2, 4	2, 1, 0	15	20	27.0	4.43	5.21
156	1, 1, 4	2, 1, 0	15	20	23.4	8.88	10.28
156	1.5, 1, 4	2, 1, 1	30	40	26.1	8.49	10.05
180	1, 2, 10	3, 2, 0	30	40	35.2	7.13	9.94

[a] Spherulite octant edge length.
[b] d = Minimum amorphous thickness; t = initial crystal thickness; and w = initial crystal width.
[c] gs = Growth step length along b; gsw = growth step along a (widening); and gst: growth step length along c (thickening).
[d] Split angle (in degrees).
[e] Splay angle (in degrees).
[f] Volume crystallinity (in per cent).
[g] Average crystal width-to-thickness ratio.
[h] Square root of the average of the square of the crystal width-to-thickness ratio.

colour. The volume crystallinity of the simulated structure was 27%, the average width attained was 12.8, with a standard deviation of 9.0; the initial value of W_i was set to 4 lattice units. The simulated structures were analyzed with regard to total crystal width of each crystal unitary block, and the widths from the central line of each block to the left-hand and right-hand periphery of the crystal blocks; the latter are referred to as the left-side and right-side widths, respectively. The distributions of right-side, left-side and overall widths for the same spherulite structure displayed in Fig. 2 are presented in Fig. 3a–c. Crystal thickening was less extensive and the increase in average crystal thickness obtained was 24%; from the initial $L_{ci} = 1$ to 1.24, with a very large standard deviation (5.0). The limited crystal thickening was due to the low value set for the growth rate along c and to

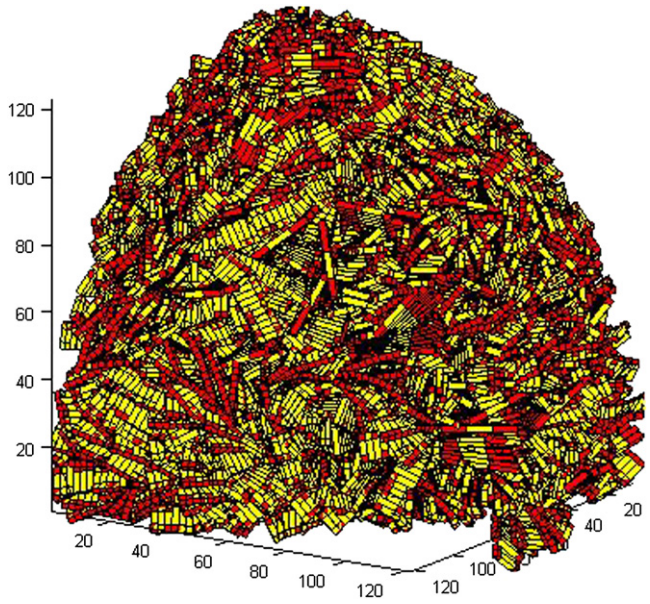

Fig. 2. A fully-grown octant of a spherulite with laterally grown crystal elements displayed in a darker (red) colour.

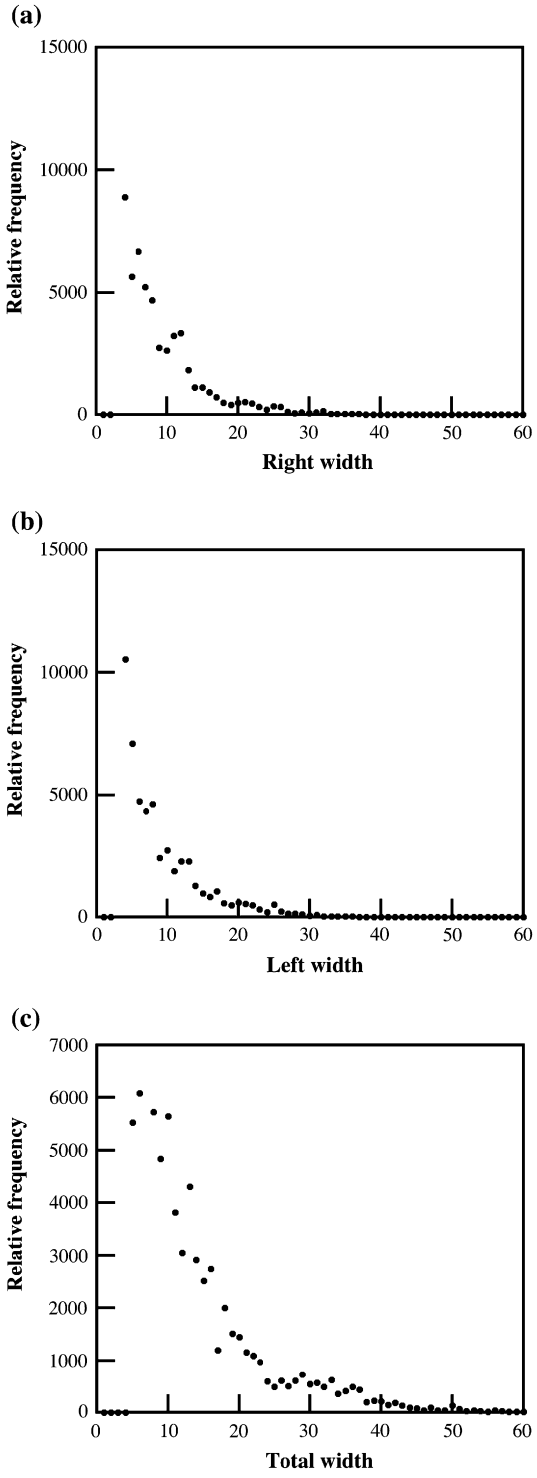

Fig. 3. Width population density in a fully-grown structure: (a) right-hand-side width, (b) left-hand-side width and (c) total width. The width of the initial crystal block was set to 4 lattice units, the lateral growth step gsw to 1 lattice unit.

the spatial limitation originating from the requirement of a minimum amorphous layer thickness. The latter principle became violated in the case of parallel stacking of the crystal lamellae. Crystal growth in all the crystallographic directions increased the crystallinity range attainable: it was possible to reach a volume crystallinity of 40% in structures while maintaining

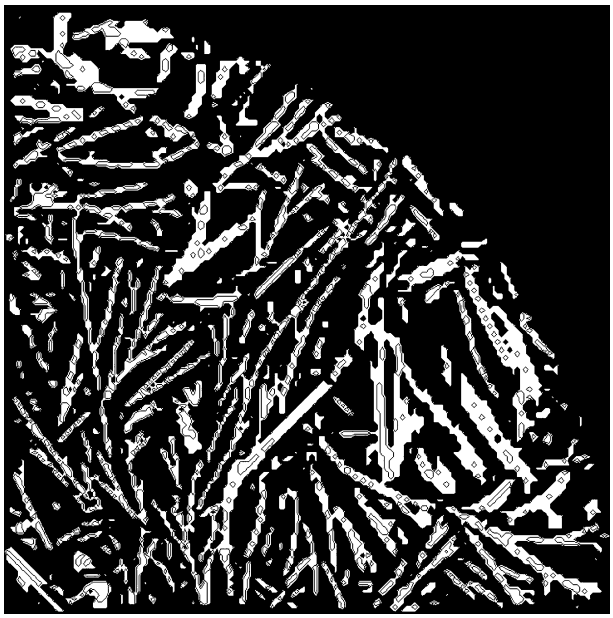

Fig. 4. Simulated transmission electron micrograph of stained structure from a mature spherulite octant. The coordinate system is scaled in lattice units.

uniform crystallinity (Fig. 4). Spherulitic superstructures have been reported for melt-crystallized polyethylene with a volume crystallinity greater than 30% [13] and thus the simulated structures are in this respect thus comparable with real structures of low crystallinity polyethylene. The crystallinity attainable is limited by the ratio of the crystal thickness to the minimum amorphous layer thickness, as was discussed by Mattozzi et al. [5].

3.2. Penetrant diffusion

Data for the spatial density of a penetrant molecule based on 100 random walks of 10^5 steps each in a spherulite octant with a cube-side length of 173 lattice points are presented in Fig. 5. Each penetrant random walk started at a random lattice site. The deviations from the expected spatial densities $D(r) \propto r^2$ and $D(t) \propto -t^2 + R^2$, where r is the radial coordinate, t the generic Cartesian coordinate (x, y or z) and R the lattice edge, are due to the blocking effect of crystals. The curves of mean-square displacement versus time for the same set of walks are shown in Fig. 6 together with the radial and tangential components of the square displacement. The higher slope of the tangential component of the square displacement is due to the double dimensionality of the movement in the plane orthogonal to the spherulite radius direction. In fact, the diffusivity was lower along the spherulite radius than in the tangential plane considering the difference in dimensionality of the two cases.

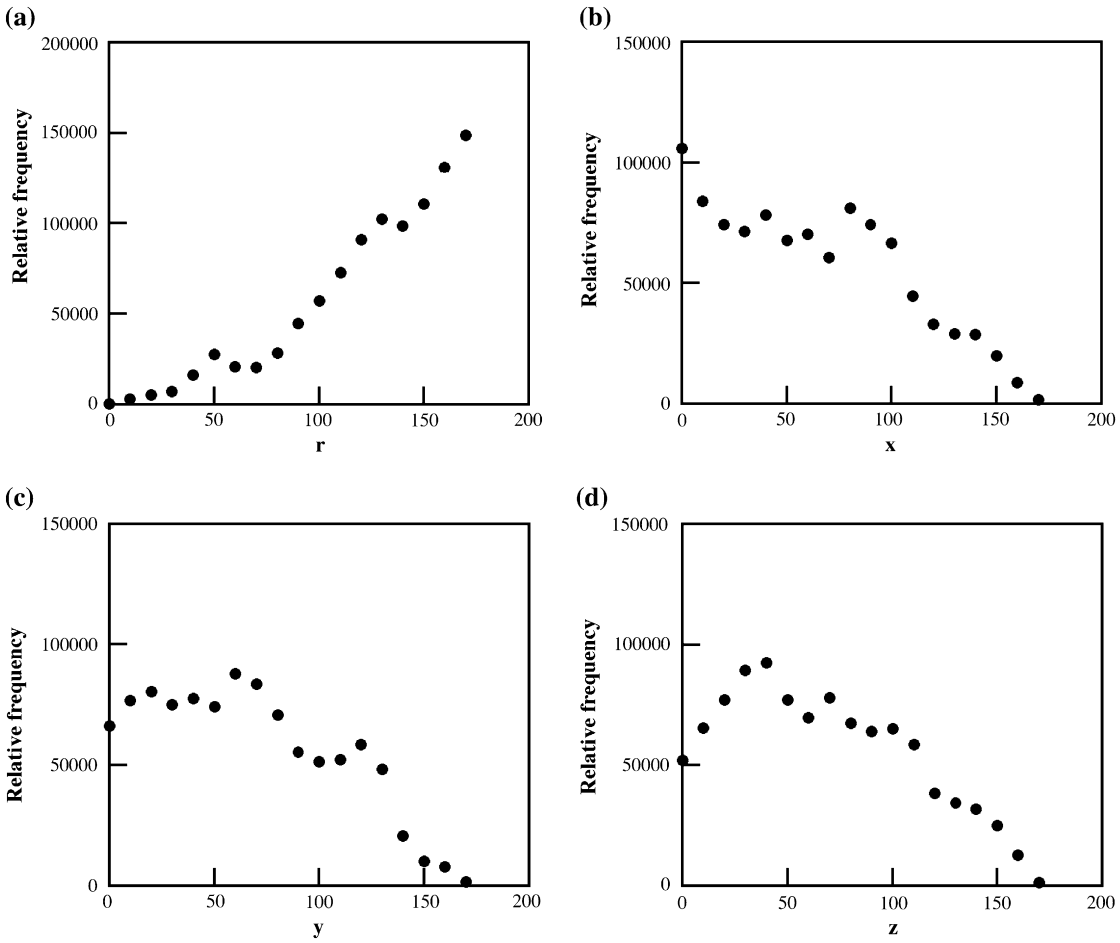

Fig. 5. Spatial density of a random walker in a spherulite octant: relative frequency of modulus of the displacement **r** and of its three components x, y and z.

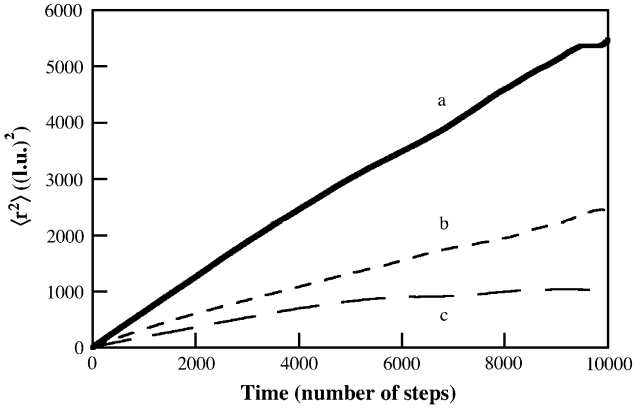

Fig. 6. Mean-square displacement $\langle \mathbf{r}^2 \rangle$ in (lattice units)^2 as a function of time (in number of steps) for a penetrant molecule making 100 trajectories, each trajectory consisting of 10^5 steps (line a; thick line). The tangential (line b) and the radial components (line c) of the square displacements sampled from the same trajectories are also shown.

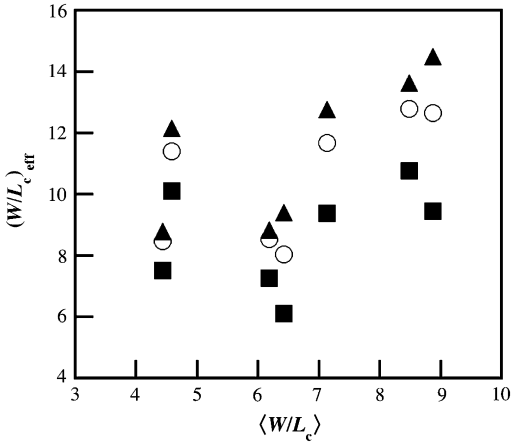

Fig. 7. The effective crystal blocking effect $(W/L_c)_{\text{eff}}$ as a function of the average of the aspect ratio $\langle W/L_c \rangle$ for a series of different simulated spherulite systems. The global crystal blocking effect (○) and its radial (■) and tangential (▲) components were calculated from the global, radial and tangential diffusivities and volume crystallinity according to Eq. (3).

The repeatability of the diffusivity determinations was assessed by running 10 replicates with 100 random walks of 10^5 steps each in the same spherulite structure and comparing the results: the standard deviation for the global, radial and tangential diffusivities were, respectively, 1.2%, 3.0% and 1.6% of the mean values, whereas the same deviations for a fully amorphous system were 1.9%, 2.6% and 1.9% of the mean values. The difference between the radial and tangential diffusivities for the amorphous octant lies within the experimental error, confirming that the periodic boundary conditions and diffusivity calculation algorithm used did not introduce any systematic anisotropic behaviour of the system.

3.3. Effect of crystal morphology on crystal blocking effect

Mattozzi et al. [5] used the formula developed by Michaels and Bixler [1]:

$$\tau_{\text{MORPH}} = 1 + \frac{v_c \left[0.384 + \left(0.785 - \left(\frac{W}{L_c} \right)^{-1} \right)^2 \right]}{1.848 - 3\left(0.785 - \left(\frac{W}{L_c} \right)^{-1} \right)^2} \qquad (3)$$

to relate the geometrical impedance factor with morphological parameters, volume crystallinity (v_c), width of crystals along the a-axis (W) and crystal thickness (L_c). Note that the geometrical impedance factor calculated from the morphological data (Eq. (3)) is designated differently (τ_{MORPH}) than that (τ_{DIFF}) calculated from the penetrant diffusivity data according to Eq. (1) with $\beta = 1$. Hadgett et al. [4] showed by Monte Carlo simulation of penetrant diffusion in computer-built structures with crystal platelets that Eq. (3) correctly described the geometrical impedance factor. Eq. (3) was thus used to estimate the effect of crystal width-to-thickness ratio on the global effective blocking factor in systems with different crystallinities (23–40%; Table 1) and different crystal morphologies (Fig. 7). Furthermore, an effective blocking factor was calculated for both the radial and tangential components of the diffusivity (Fig. 7).

The global and tangential blocking factors showed the strongest increase with increasing average lamellar width-to-thickness ratio, whereas the radial effective blocking factor displayed a more moderate increase with increasing crystal aspect ratio. The crystal lamellae blocked penetrant motion in the tangential plane more efficiently than along the spherulite radius. The crystal cross-section along a vector in the tangential plane should be greater than that along the spherulite radius (cf. Fig. 4), which is in accordance with the following findings: the angle between the crystallographic b-axis and the spherulite radius was, on an average for all simulated spherulites, equal to ca. 25°; the average values for individual spherulites (of different degrees of crystallinity and crystal width-to-thickness ratio) varied between 22.9° and 28.7°. The a- and c-crystal directions were on an average perpendicular to the spherulite radius. The crystal directions were essentially the same and independent of radial position in the spherulite. It should be noticed that the diffusion was simulated on-lattice and that all penetrant jumps, except those at the edge of the octant and parallel to it, contain both a radial and a tangential component. Hence, two components of the diffusivity are correlated.

Fig. 8 shows that the data for the geometrical impedance factor (τ_{DIFF}) obtained from diffusivity data according to Eq. (1) are not in accordance with the Fricke theory using the average data for W/L_c as inputs in Eq. (3). For a certain value in $\tau_{\text{MORPH}} = 1.4 \pm 0.1$, τ_{DIFF} shows a variation between 1.2 and 1.9. The data points in the low value range are from Mattozzi et al. [5] for low crystallinity samples ($v_c = 10$–14%) with a uniform W/L_c-value. The highest value obtained for τ_{DIFF} is for the system with the highest attained crystallinity, $v_c = 40\%$. By using another average for W/L_c based on the square of this quantity the data points associated with systems with wide distributions in W/L_c were shifted along the x-axis towards $\tau_{\text{DIFF}} = \tau_{\text{MORPH}}$ and a rectilinear trend in the data was obtained for systems of intermediate degree of crystallinity

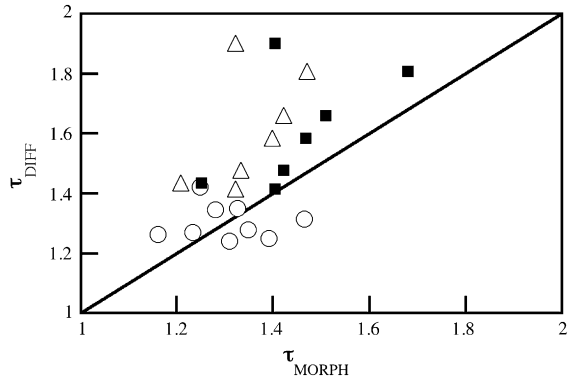

Fig. 8. Geometrical impedance factor (τ_{DIFF}) calculated from Eq. (1) as a function of the geometrical impedance factor (τ_{MORPH}) calculated from morphological data according to the Fricke theory (Eq. (3) for the following different spherulitic systems: spherulites with constant W/L_c (○); spherulites with a distribution in W/L_c, the arithmetic mean of W/L_c was used in the calculation of τ_{MORPH} (△); spherulites with a distribution in W/L_c, the arithmetic mean of the square of W/L_c was used in the calculation of τ_{MORPH} (■).

(17–35%). The average slope of these data points was 1.43 which corresponds to an increase in the effective W/L_c ratio by a factor of 1.5 ± 0.1. Both systems with very low degree of crystallinity and most notably the system with the highest crystallinity showed important deviations from this trend. The system with the highest crystallinity showed a τ_{DIFF} of ca. 1.9 which was 0.5 higher than expected from the general trend. The following general conclusions can be drawn from these data:

- Wider crystals are significantly more effective than smaller crystals in blocking the penetrant diffusion. Experimental data [14] show that Eq. (3) lacks accuracy when predicting crystal blocking effects for materials with a high crystal width-to-thickness ratio; the source of the error may well be the systematic underestimation of the crystal blocking effect if the arithmetic mean is used to define the crystal width-to-thickness ratio distribution. The results show that, besides the volume crystallinity and the width-to-thickness ratio average, the distribution of the crystal width-to-thickness ratio is important by itself and has to be considered when assessing the transport properties of semicrystalline polymers with spherulitic superstructure.
- Systems of intermediate volume crystallinity (17–35%) conformed to a trend, which could be described by the Fricke equation provided that it included a factor (ca. 1.5) multiplying the actual W/L_c ratio; the latter being based on the quadratic mean value.
- The system with the highest degree of crystallinity ($v_c = 40\%$) showed a significant deviation from the general trend with a markedly higher measured geometrical impedance factor than predicted by the Fricke theory or even with respect to a modified version of the theory (i.e. assuming a factorial increase in W/L_c by ca. 1.5). It is thus relevant to study spherulites with a volume crystallinity greater than 40% and to establish the relationship between τ_{DIFF} and τ_{MORPH} for these systems.

4. Conclusions

The algorithm generating spherulite-like arrangements of crystal lamellae developed in a previous work was refined to permit crystal widening and thickening. Lateral growth of the lamellae increased the range of attainable crystallinities up to 40% (from maximum 35% in spherulites with constant crystal width and thickness), notwithstanding the limitations due to system size. Lamellar thickening occurred to a lesser extent, due to spatial confinement appearing in the case of parallel stacking of lamellae. Spherulites with a uniform crystallinity and crystal width-to-thickness ratio up to 35 were obtained. The penetrant trajectories based on an on-lattice Monte Carlo algorithm showed that the crystals hindered diffusion mostly perpendicular to the spherulite radius. The smaller crystal blocking of diffusion along the spherulite radius was due to the presence of crystals with their *b*-axes predominantly oriented along the spherulite radius. For systems with a wide distribution in crystal width-to-thickness ratio the average of the squares of this parameter is more suitable than the normal average to use in the calculation of the geometrical impedance factor according to the Fricke model. Systems of intermediate volume crystallinity (17–35%) conformed to a trend, which could be described by the Fricke equation provided that it included a factor (ca. 1.5) multiplying the actual W/L_c ratio; the latter being obtained as the square root of the quadratic average. Most interestingly, the system with the highest volume crystallinity (40%) showed a markedly higher geometrical impedance factor than predicted by the Fricke theory using the two modifications, quadratic mean and the 1.5-factor.

Acknowledgements

The financial support from the Swedish Research Council (grant # 5104-20005764/20) is gratefully acknowledged.

References

[1] Michaels AS, Bixler HJ. J Polym Sci 1961;5:413.
[2] Fricke H. Phys Rev 1924;24:575.
[3] Müller-Plathe F, Rogers SC, Gunsteren WFv. Macromolecules 1992;25:6722.
[4] Hadgett PM, Goldbeck-Wood G, Windle AH. Polymer 2000;41:6151.
[5] Mattozzi A, Serralunga P, Hedenqvist MS, Gedde UW. Polymer 2006;47:5588.
[6] Bassett DC. J Macromol Sci Phys 2003;B42(2):227.
[7] Keith HD, Padden FJ, Lotz B, Wittman JC. Macromolecules 1989;22:2230.
[8] Kanig G. Kolloid Z Z Polym 1973;251:782.
[9] Bassett DC. CRC Crit Rev 1984;12:97.
[10] Bassett DC, Olley RM. Polymer 1984;25:935.
[11] Bassett DC, Vaughan AS. Polymer 1985;26:717.
[12] Einstein A. Ann Phys 1905;17:549.
[13] Bensason S, Minick J, Moet A, Chum S, Hiltner A, Baer E. J Polym Sci Polym Phys 1996;34:1301.
[14] Mattozzi A, Neway B, Hedenqvist MS, Gedde UW. Polymer 2005;46:929.